International Journal of Pharmaceutics 618 (2022) 121663

Contents lists available at ScienceDirect

International Journal of Pharmaceutics

journal homepage: www.elsevier.com/locate/ijpharm

Proof of concept of a predictive model of drug release from long-acting implants obtained by fused-deposition modeling

Giuseppe Manini [a,b,*], Samira Benali [b], Jean-Marie Raquez [b], Jonathan Goole [a]

[a] Laboratory of Pharmaceutics and Biopharmaceutics, Université libre de Bruxelles, Campus de la Plaine, CP207, Boulevard du Triomphe, Brussels 1050, Belgium
[b] Laboratory of Polymeric and Composite Materials (LPCM), Center of Innovation and Research in Materials and Polymers (CIRMAP), University of Mons, Place du Parc 23, B-7000 Mons, Belgium

ARTICLE INFO

Keywords:
3D printing
Paliperidone palmitate
Design of experiments
Predictive models
Personalized medicine
Hot-melt extrusion
Fused deposition modelling

ABSTRACT

In the pharmaceutical field, there is a growing interest in manufacturing of drug delivery dosage forms adapted to the needs of a large variety of patients. 3D printing has proven to be a powerful tool allowing the adaptation of immediate drug delivery dosage forms. However, there are still few studies focusing on the adaptation of long-acting dosage forms for patient suffering of neurological diseases. In this study, paliperidone palmitate (PP) was chosen as a model drug in combination with different polymers adapted for fused-deposition modeling (FDM). The impact of different printing parameters on the release of PP were investigated. The layer thickness and the infill percentage were studied using a quality by design approach. Indeed, by defining the critical quality attributes (CQA), a proof of concept of a prediction system, and a quality control system were studied through designs of experiments (DoE). The first part of this study was dedicated to the release of PP from a fix geometry. In the second part, the prediction system was developed to require only surface and surface to volume ratio. From that point, it was possible to get rid of a fix geometry and predict the amount of PP released from complex architectures.

1. Introduction

The versatility of 3D printing technology allows adapting pharmaceutical dosage forms to specific populations of patients. Indeed, the shapes can be printed so as to mimic "sweet-like" chewable tablets, it can be topped with Braille pattern or even adapted for older patients (Scoutaris et al., 2018; Awad et al., 2020). The shape and the design of a dosage form can be easily adapted and improved thanks to the needs of patients and/or the treatment of pathologies. For instance, the pattern of the dosage form can be modulated to increase the ease of picking and the swallowing for elderly patients (Goyanes et al., 2017).

However, the interest in 3D printing of pharmaceutical dosage forms can go further. The preparation of different printed dosage forms does not require any adaptation of the formulation. Only one formulation can be used to create different medicines and thereby achieving different release profiles from a unique starting material (Manini et al., 2021).

In order to achieve this customization, modifications can be done throughout the 3D printing process, starting from the computer-aided design (CAD) software to the printing parameters. Indeed, the overall design of the printed part can be modulated using a CAD software. *Goyanes et al.* studied the dissolution profiles of an acetaminophen-loaded polyvinyl-alcohol 3D dosage form with different geometries: cubes, pyramids, torus, cylinders and spheres. The modification of the surface, the volume and the surface to volume ratio allowed obtaining different release profiles of the drug (Goyanes et al., 2015).

Complex structures can also be used to improve the properties of available design. In this way, *Saida and coworkers* introduced a new design of capsules containing built-in channels to accelerate the release of hydrochlorothiazide. The impact of the channel width, their length and position were investigated in addition to the influence of the surface area to volume ratio on the drug release profile. The complex structure proposed by *Sadia et al.* did not only increased the surface area of their

Abbreviations: ANOVA, analysis of variance; CAD, computer aided design; CQA, critical quality attributes; *D*, dispersity; DSC, differential scanning calorimetry; DoE, design of experiment; EVA, ethylene vinyl acetate; FDM, fused deposition modeling; GPC, gel permeation chromatography; HME, hot-melt extrusion; IC95, interval of confidence 95%; M_w, molecular weight; PCLLA, PCL-Co-La; PLA, poly(lactic acid); PP, paliperidone palmitate; QbD, quality by design; S/V, surface to volume ratio; T_g, glass transition; TGA, thermogravimetry; XRD, X-Ray diffraction.

* Corresponding author.
E-mail address: giuseppe.manini@ulb.be (G. Manini).

https://doi.org/10.1016/j.ijpharm.2022.121663
Received 27 December 2021; Received in revised form 8 March 2022; Accepted 9 March 2022
Available online 12 March 2022

capsules, but also increased the diffusion of the medium through the dosage form (Sadia et al., November 2017).

Furthermore, the possibilities for modulating the release profile using 3D printing do not end at the overall design. Indeed, after creating the general design of the model, the software generates a.stl file. This file cannot be read by the 3D printer and requires a second software which is able to generate a.gcode file. During the use of this second software, other modifications can be applied to the general design of the printed part. For instance, it is possible to modulate parameters, such as the layer thickness, as well as the percentage of infill. *Fanous and coworkers* produced Eudragit® EPO-based 3D printed printlets loaded with lumefantrine for pediatric patients. Printlets were designed with different infill densities, ranging from 65 to 100 % v/v. They observed a significantly highest drug release from printlets with an infill density of 65 % v/v (Fanous et al., 2021). In another study, *Thakkar et al.* investigated the influence of the infill percentage on *in vitro* performance of 3D printed printlets. The dosage forms were prepared using an ibuprofen-loaded filament based on hydroxypropyl methylcellulose acetate succinate. Infill percentages ranging from 20 to 80 % v/v were evaluated. Through the *in vitro* dissolution test, the percentage of drug release over time was reduced with the increase of the density (Thakkar et al., 2020).

Indeed, controlling the drug release profile is essential to prepare patient-specific dosage forms. However, there are still few studies focusing on long-acting dosage forms and the prediction of drug released based on a selected design.

Design of Experiments (DoE), a component of the Quality by Design (QbD) approach, was used to improve the understanding of inputs parameters on different responses. In the first part of this study, the infill and the layer thickness were characterized as critical quality attributes (CQA) of the amount of PP released over time. The surface, volume and the weight of the personalized dosage forms were evaluated as well as the amount of PP released through an *in vitro* dissolution test.

In the second part of this work, the release of PP from complex structure was studied. A second DoE was performed in which the CQAs were based only on the surface area, the volume and the ratio of both parameters. The use of these input parameters allowed getting rid of a fixed geometric shape. In addition, the release profile of PP was modulated using a dual printer head allowing the preparation of dosage forms based on two PP-loaded formulations.

2. Materials and methods

2.1. Materials

PLA 4060D, amorphous PLA with 12 % D-Lactide, was purchased from Ingeo NatureWorks® (USA) (Llc, 2005), EVA 233 with 23 % of vinyl acetate content was purchased from Exxon Mobil Chemical Company®(USA). CAPA 8502, a copolyester of PCL-Co-LA based on 90 % w/w of PCL and 10 % w/w of lactide was purchased from Perstorp® (Sweden). Paliperidone palmitate was purchased from Biochem Partner (China). Trifluoroacetic acid, chloroform, chloride methylene, acetonitrile and isopropanol were purchased from Sigma-Aldrich® (USA). Hydrochloric acid and Tween® 20 were purchased from VWR® (USA).

Table 1
Formulation compositions.

Formulation Names	PLA % (w/w)	EVA % (w/w)	PCLLA % (w/w)	PP % (w/w) Theoretical	PP % (w/w) Experimental (Mean ± SD, n = 3)
PLA_EVA_PP	72	18	/	10	9.8 ± 0.3
PLA_PCLLA_PP	67.5	/	22.5	10	9.7 ± 0.2

2.2. Preparation of drug-loaded formulations

2.2.1. Composition of studied formulations

In this study, two formulations were studied (Table 1).

The preparation of the filaments was done through a pre-formulation step between the PLA with the EVA or with the copolymer of caprolactone and lactide (PCLLA). After this first pre-formulation step, both blends were ground to obtain a fine powder. Then, the PP was added, and a cryogenic milling step was carried out on the mixtures allowing an intimate mixing of the different elements. At the end, an extrusion step was performed on the formulation to obtain a homogeneous filament adapted to the 3D printer.

2.2.2. Cryogenic milling

Cryogenic milling was conducted in an oscillatory Retsch® Cryomill (Retsch GmBH©, Haan, Germany). The formulations were placed in a 25 ml stainless steel grinding jar with 3 stainless steel beads of 15 mm. The milling time was divided into different cycles of 2 min at 30 Hz and different cycles of 30 s at 5 Hz to avoid any overheating. The cryogenic milling was carried out on formulations to reduce the aggregates into powder. Then, formulations were passed through a 40 mesh sieve.

2.2.3. Hot-melt extrusion process (HME)

Drug loaded filaments were prepared by HME using a parallel twin-screw extruder (Thermo Scientific® Process 11, Thermo Fisher Scientific Inc.®, USA) with 8 separate heating zones, including the die (ø = 1.75 mm). Temperature, die pressure, torque, and speed of rotation of the screws were continuously monitored. The speed of the screws was fixed at 30 rotations per minute (RPM). The temperature of the different heating zones was fixed as follow (from zone 1 to zone 8): 60/80/125/125/125/125/125/110 °C. A volumetric feeder (Volumetric Mini Twin-Feeder, Thermo Fisher Scientific Inc.®, USA) was used to convey the formulation into the extruder and the screw speed of the feeder was set at 5 RPM. After extrusion, the filament was collected using a filament winder to obtain a diameter of 1.75 ± 0.1 mm.

2.3. Characterization methods

2.3.1. Thermal analysis

Differential scanning calorimetry (DSC) was conducted with a DSC Q2000 with T_{zero} Technology and RCS cooling system. Temperature and enthalpy calibrations were performed using an indium standard (TA Instruments®, New Castle, USA). Approximately 5–10 mg of samples were sealed in T_{zero} hermetic aluminum pan. The samples were heated from −50 to 130 °C with a heating rate of 10 °C/min. All analyses were conducted under nitrogen atmosphere (50 ml/min).

Thermal decomposition of samples was assessed by thermogravimetric analysis (TGA). The analysis was performed with a TGA Q500 (TA Instruments®, New Castle, USA). Samples of 5–10 mg were loaded into a platinum pan and were heated from 30 to 450 °C with a heating rate of 10 °C/min under nitrogen gas (flow rate: 60 ml/min).

2.3.2. Gel permeation chromatography (GPC)

GPC analysis was conducted on an Agilent liquid Chromatography (Agilent Technologies®, United States) equipped with an Agilent degasser, an isocratic HPLC pump with a flow rate set at 1 ml/min. Chloroform was used as mobile phase and polystyrene were used as standards for calibration. The GPC was equipped with an Agilent autosampler, the loop volume was 100 µL. The solutions were concentrated at 2 mg/ml. The GPC was equipped with an Agilent DRI refractive index detector and three columns: a PL gel 5 mm guard column (Polymer Laboratories®, Ltd, United Kingdom) and two PL gel Mixed-B 5 µm columns (columns for separation of polystyrene with a M_w ranging from 200 to $4x10^5$ g/mol) were used at 30 °C to evaluate the M_w of samples.

2.3.3. X-ray powder diffraction (XRD)

A powder X-Ray diffractometer (D8 Advance Eco Bruker®, Madison, USA) equipped with a one-dimensional silicon detector (LynxEye, Bruker AXS) was used to characterize the crystalline/amorphous structure of PP, starting elements and formulations. Using a Cu Kα radiation (1.54 Å; 40 kV × 25 mA) data were collected, over the angular range of 3-45° 2θ and a step size of 0.02° and a dwell time of 1 s.

2.3.4. Determination of drug loading

To extract the PP, samples loaded with an average weight of 1 mg of PP were solubilized in 1 part v/v of chloride methylene under vortex until its complete solubilization. Then, 9 parts v/v of isopropanol were added drop by drop under vortex. Solutions were filtered through 0.22 µm filters (Sortorius®) and filled in 2 ml vial for HPLC analysis.

A HPLC-UV method was conducted to evaluate the drug loading from 3D implants. Mobile phase A, which consisted of acetonitrile (100 % v/v), and mobile phase B (aqueous solution of trifluoroacetic acid at pH 2) were used at ratio 70/30 A/B (v/v). The flow rate was set at 1 ml/min for 20 min and the wavelength was fixed 278 nm. The retention time of PP was 8.0 min.

2.4. 3D printed dosage forms

2.4.1. Design software and studied designs

Tinkercad® was used as computer aided design (CAD) program to design the geometry of proof of concept dosage forms. The generated CAD files were converted into.stl files. Then, the obtained files were imported into an open-source software for slicing before printing. Ideamaker® software, was used to generate.gcode files compatible with the 3D printer.

2.4.2. Designs of dosage forms studied in part I & II

The design and dimensions of the dosage forms used in Part I & II represented in Fig. 1 were established using Tinkercad™.

2.4.3. In vitro dissolution test

After their printing, the 3D printed dosage forms were placed in 5 ml transparent vials and filled with 1.5 ml of dissolution medium which consisted of 2 % (w/w) Polysorbate 20® in 0.001 N HCl as adapted from the guidance published by the Food and Drug Administration (Dissolution Database for PP) (Database, 2021). The vials were placed in a GFL® (Burgwedel, Germany) water bath kept at 37 °C. The *in vitro* dissolution test of 3D dosage forms was evaluated over a period of 1 month. During this period, the medium was replaced at each sampling time to maintain sink conditions.

2.5. Fused deposition modeling (FDM)

3D printed dosage forms were obtained using a Raise3D® Pro2 (Irvine, USA) as the 3D printer. The printing temperature was set at 150 °C, the bed temperature at 55 °C, the flow rate at 120 %, the printing and infill speed were set at 30 mm/s for both formulations. During the 3D printing, no top or bottom layers were applied on the 3D design to distinguish the impact of the infill.

2.6. Design of experiments (DoE)

All the experiments were planned using Design Expert® 12 software (Stat-Ease®, Minneapolis, USA) and the models were examined using one-way analysis of variance (ANOVA). The factors and levels considered in the experimental designs are presented in Table 2. In the first experimental design, the layer thickness and the infill parameter were investigated. In the second experimental design, the volume and surface to volume ratio were studied as factors. I-optimal design was carried out to identify possible interactions between the factors on the release of PP overtime. The best fitting models were selected based on their F and p-values for each response. Model terms were considered as significant when F-values were greater than 1 and p-values lower than 0.05.

2.7. Statistical data analysis

All experiments were performed in triplicate, unless otherwise mentioned. Prism 7 software (GraphPad® software, USA) was used for statistical analysis. Statistical analysis to evaluate significant differences between the different dissolution profiles was performed using student *t*-test. The level of significance was accepted at $p < 0.05$.

2.8. Surface and volume measurement

Among the parameters evaluated in this study, the surface area, the volume and their ratio were evaluated for the different 3D printed dosage forms. This analysis was performed using the Meshmixer® program on.stl files. However, after the modulation of the infill and the layer thickness by the slicer,.gcode files were produced and cannot be opened by Meshmixer®. In order to overcome this problem, the.gcode files were transformed into.stl files through the use of the Voxeliser® program. This transformation allows the evaluation of the surface and the volume of the 3D parts after modulation of the infill and the layer thickness.

3. Results and discussion

3.1. Preparation and characterization of printable filaments

The first part of this work consisted of preparing the 3D printed dosage forms. Various subsequent steps were mandatory to achieve the 3D printing process, such as the characterization of the raw materials and the manufacture of the filaments by HME.

The raw elements (Table 1) were characterized by DSC, TGA and XRD. The information provided by these analyzes allowed the

Table 2
Factors and levels applied in the experimental designs.

	Factors	Levels
1st experimental design	Layer thickness (µm)	100, 200, 300
	Infill (%)	0, 25, 50, 75, 100
2nd experimental design	Volume (mm^3)	40, 60, 80
	Surface to volume ratio (mm^2/mm^3)	2, 4, 6

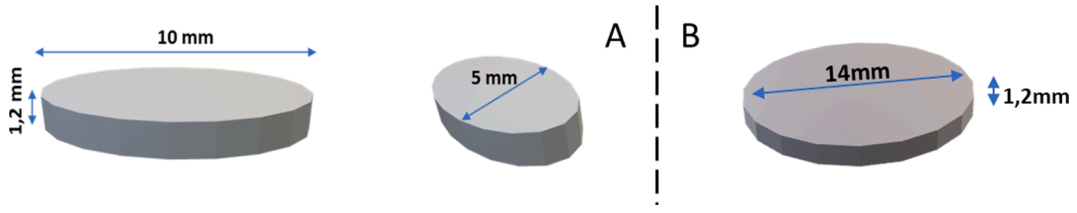

Fig. 1. A) Implant design studied in Part I: Length 10 mm × Width 5 mm and Height 1.2 mm. B) Implant design studied in Part II: Diameter 14 mm × Height 1.2 mm.

assessment of their thermal properties, thermal stability as well as their crystalline or amorphous state.

In order to erase the thermal history of the starting components, DSC analyzes were carried out on the second heating cycle (Fig. 2). PLA 4060D, due to its amorphous nature, only showed a Tg at 59 °C. EVA and PCLLA showed a melting range between 60 and 80 °C for EVA and at 45 °C for PCLLA. On the other hand, after a first heating cycle which was followed by a cooling cycle, the PP was in its amorphous form with a cold crystallization temperature at 56 °C and a melting point at 114 °C. Then, the thermal stability was assessed by TGA (Fig. 3).

From the TGA results, it could be observed there was no mass loss until 300 °C for the different polymers investigated herein. On the other hand, the PP started its decomposition at 200 °C. Indeed, the results observed on the first derivative showed a first mass loss starting from 200 °C with a maximum degradation peak at 300 °C.

In this study, EVA and PCLLA were used to reduce the extrusion temperature of PLA4060D. Indeed, the presence of 18 % w/w EVA or 22.5 % w/w PCLLA allowed the extrusion of mixtures containing more than 65 % w/w PLA at a temperature of 125 °C. This decrease of the extrusion temperature was essential to preserve the integrity of the PP during the entire process. Indeed, the extrusion temperature of PLA 4060D alone is ranging between 180 °C and 210 °C[10]. However, this temperature was too close to the degradation temperature of PP. After thermal characterization of the various compounds, XRD analysis was carried out on the elements before extrusion and after 3D printing (Fig. 4).

No diffraction peak was observed for PLA and EVA. On the other hand, PCLLA showed two Braggs peaks at 21.4 and 23.8°, which was ascribed to the diffraction peaks of crystallographic lattices of PCL (Li et al., 2010; Cheng et al., 2009; Holländer et al., 2016; Manini et al., 2021). Indeed, the PCLLA used in this study was composed at 90 % w/w of PCL. The PP, in its crystalline state before process, showed many diffraction peaks including two intense signals at 5.7 and 7.8° (Manini et al., 2021; Leng et al., 2014). Since neither PLA, EVA nor PCLLA present any diffraction peaks between 4° and 8°, the presence or absence of both main PP peaks in this range was used to attest the crystalline or amorphous state of the drug after 3D printing.

After the different characterizations, an extrusion step was carried out on both formulations to produce filaments with a constant diameter of 1.75 ± 0.1 mm. After having physically mixed the pre-formulations and the PP using a mortar and a pestle for 5 min, cryogenic milling was carried out on both mixtures. The purpose of a milling stage allows a reduction of residual agglomerates and intimately blend the different components of the formulation (Allaf et al., 2019). In addition, a milling stage using liquid nitrogen avoids the risk of an overheating that may induce a degradation of the components. Then, the formulations were placed in the feeder of the extruder. The speed of the extruder as well as the feeder and the winder were optimized to obtain a filament with of 1.75 ± 0.1 mm diameter.

3.2. Part I - investigation of 3D printing parameters affecting the release of paliperidone palmitate

The first part of this work was dedicated to the discrimination of parameters having an impact on the release of PP over time. The influence of the infill and the layer thickness was evaluated. The dosage forms were designed to get 10 mm in length, 5 mm in width and a height of 1.2 mm (Fig. 1, A). The length, width and height of the dosage forms have been fixed. The infill was modulated to assess its impact on the surface and volume of the overall dosage form. Indeed, most commercially available subcutaneous implants such as Norplant™ or Viadur™ were designed with a cylindrical shape allowing an easier surgical implantation. However, by modeling a flattened dosage form, it was easier to highlight the effect of the infill on the surface and volume of the printed dosage forms.

3.2.1. DoE - layer thickness and infill percentages

The layer thickness and the infill percentage were used as discrete factors in the DoE. In order to assess the impact of these factors during the *in vitro* dissolution test, three different layer thicknesses were evaluated in this study: 100, 200 and 300 µm. At the same time, five infill percentages were studied: 0, 25, 50, 75 and 100 % v/v (Fig. 5).

From both discrete parameters, 18 runs were defined by the Design Expert® program (Table 3). The runs were divided in two blocks as all the runs could not be printed at once and required the stop and restart of the 3D printer.

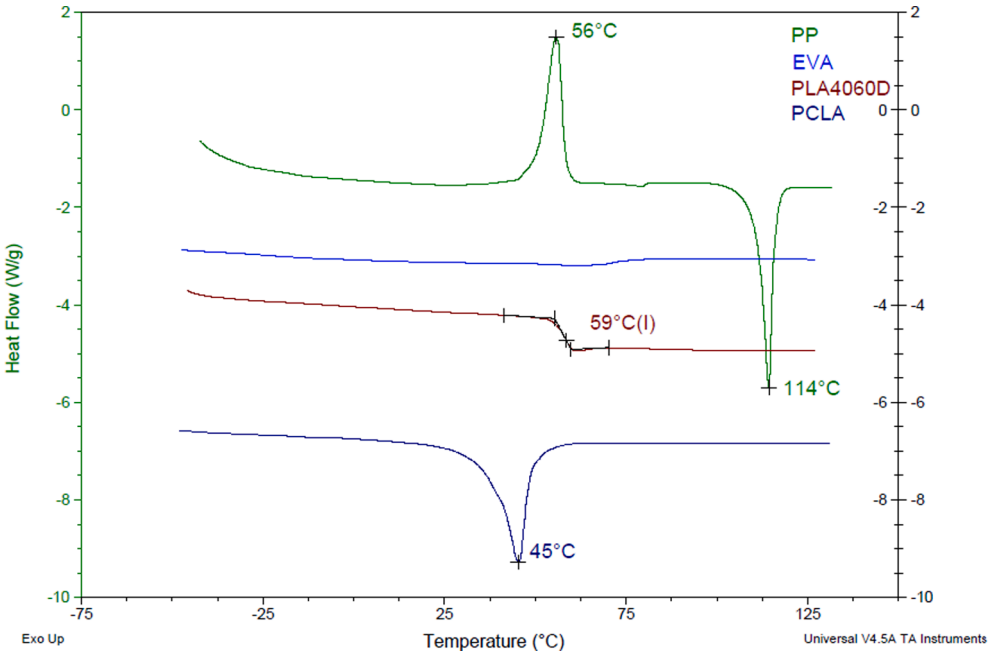

Fig. 2. DSC analysis of raw materials (analysis on 2nd heat cycle, heating rate 10 °C/min).

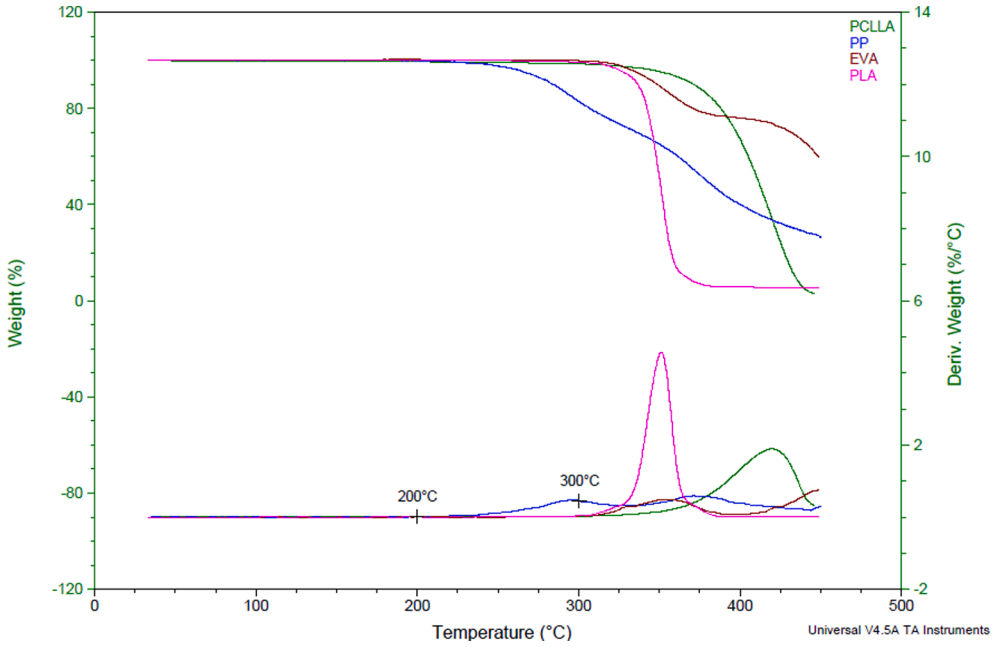

Fig. 3. TGA analysis of starting elements presented as weight loss (%) (UP) and its first derivative (DOWN) with a heating rate of 10 °C/min under nitrogen (TGA Q500 - flow rate: 60 ml/min).

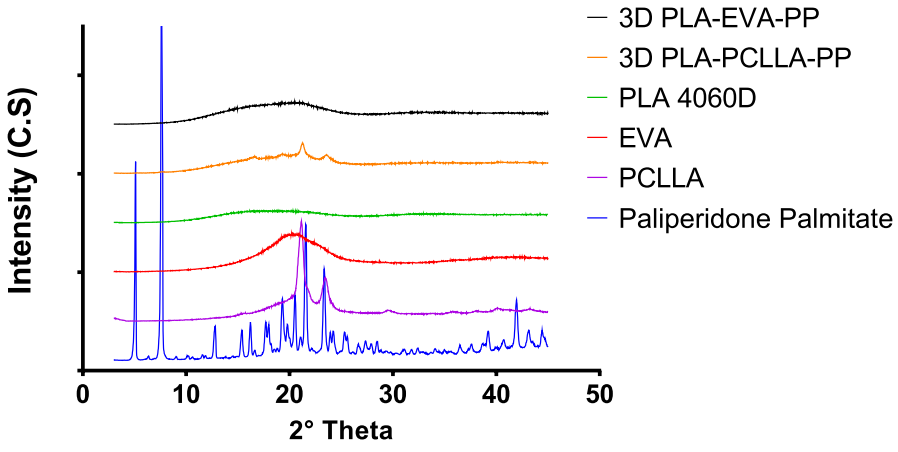

Fig. 4. XRD analysis of raw materials and 3D printed formulations (PLA-EVA-PP and PLA-PCLLA-PP).

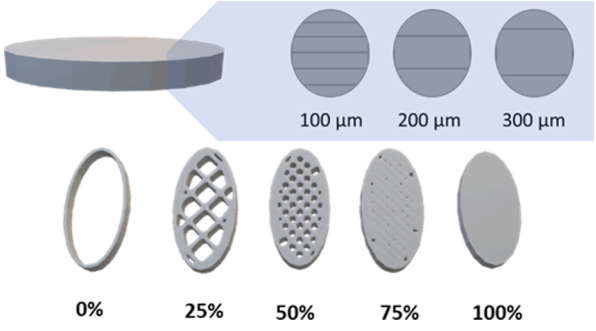

Fig. 5. Up) Three layer thicknesses assessed: 100, 200 and 300 µm. Down) Infill percentages investigated (from left to right): 0, 25, 50, 75 and 100 %.

3.2.2. Characterization and in vitro dissolution test of 3D printed dosage forms

After designing the dosage form via Tinkercad®, the.stl file was sent to the Ideamaker® program, allowing the modulation of infill and layer

Table 3
Design of Experiments (DoE).

	Run	Infill %	Layer µm
Block 1	1	100	100
Block 1	2	0	200
Block 1	3	0	100
Block 1	4	100	300
Block 1	5	50	100
Block 1	6	25	300
Block 1	7	0	200
Block 1	8	0	100
Block 1	9	100	100
Block 1	10	25	300
Block 1	11	100	300
Block 2	12	25	200
Block 2	13	25	100
Block 2	14	75	200
Block 2	15	0	300
Block 2	16	50	200
Block 2	17	100	200
Block 2	18	50	200

thickness according to Table 3. Then, the files were saved as.gcode and used by the 3D printer. The different runs listed in Table 3 were printed using the PLA-EVA-PP formulation (Fig. 6). Using the Raise 3D Pro2®, the 3D printed dosage forms were successfully printed at 150 °C. In order to increase the adhesion of the first layers, the 3D printer bed was heated at 55 °C. After printing, XRD analysis was carried out on 3D printed dosage forms to evaluate the amorphous or crystalline state of PP (Fig. 4). The results showed the disappearance of the crystalline PP diffraction peaks between 4° and 8°, assuming the creation of the amorphous state of PP. Indeed, it has already been shown in a previous study that the extrusion and 3D printing of PP allowed the obtention of its amorphous form (Manini et al., 2021).

Throughout the printing stage, no top or bottom layers were applied to the dosage forms. During 3D printing, the infill is generally used to reduce the amount of material needed inside the printed parts allowing a reduction of the printing time, material cost and lighter printed parts. By removing the top and bottom layers, the infill has a direct impact on the surface and the volume of the dosage form. In addition, during an *in vitro* dissolution test, the dissolution medium can be directly in contact with the entire surface of the printed dosage form.

The different types of 3D printed devices obtained by the Raise3D Pro2® can be shown in Fig. 6. It can be noticed that 0 % v/v of infill corresponded to an empty or hollow 3D form, while 100 % v/v of infill corresponded to a monolith. However, there was a wide possibility of variation between both values. Indeed, when the 3D dosage forms were printed with an infill of 25 % v/v, the implants had a higher porosity and surface than the monolith. As the infill increased, the number of printed meshes increased and the area of the pores created by the deposited materials was getting smaller. *Zhang et al.* evaluated the impact of infill ranging from 20 to 70% v/v on the pore area of 3D printed erodible pharmaceutical dosage forms. The surface area of the interfilamentous gap from 3D printed elliptical tablets were observed using SEM images. The experimental data were fitted with the theoretical one and a power law correlation with a R^2 of 0.98 was obtained between the infill and the pore area (Zhang et al., 2021).

Increasing the infill percentage increased the amount of deposited material until the juxtaposition of the deposited layers leading to the obtention of a monolith at an infill of 100 % v/v. Therefore, the surface and the volume were modified by varying the infill parameters. Concomitantly, the impact of the layer thickness on the drug release was also studied in this first part. Indeed, as it was already demonstrated, this parameter may influence the mechanical properties of 3D printed parts (Carlier et al., 2019), which can also have an effect on drug release (Nober et al., 2019).

After their printing, the weight, the surface, the volume, the surface/volume ratio as well as the quantity of PP released over 1 month were evaluated. In order to obtain the information related to the surface area and the volume, Meshmixer® program was used to analyze the.stl files corresponding to each run listed in Table 3.

The values were subsequently analyzed with Design Expert® (Fig. 7).

Fig. 6. 3D printed implants with different infills, from left to right, 0, 25, 50, 75 and 100 % with a layer thickness of 200 μm.

Using this program, randomized response surface models were investigated to discriminate the impact of the infill percentage and the layer thickness on the total weight, surface, volume and S/V ratio of 3D printed dosage forms. Then, a regression analysis was carried out on the obtained responses. An ANOVA was performed to determine if the initial parameters had a significant effect ($p < 0.05$) as well as any possible interaction (Table 4).

From the ANOVA, a quadratic model was applied for the surface and volume analysis. On the other hand, a linear model was applied for the S/V ratio and for the total weight analysis.

A linear relationship was obtained between the infill, the layer thickness and the total weight of the 3D printed dosage forms with a R^2 of 0.903 (Fig. 7, A). Indeed, the amount of deposited material by the 3D printer was directly related to the infill percentage. This effect can be clearly observed when no top or bottom layers were applied to the 3D printed dosage forms (Fig. 6). Comparatively, *Zhang et al.* also evaluated the impact of the infill on the weight of 3D printed tablets and found a linear correlation between them ($R^2 = 0.9951$). Comparatively to the results obtained for the total weight, the volume also increased in correlation with the infill. This growth was described by a power law correlation ($R^2 = 0.999$) (Fig. 7, B).

On the other hand, the results obtained for the evaluation of the total surface did not correspond to a linear correlation. Indeed, a maximum surface area was obtained for an infill ranging between 50 and 75 % v/v, while minimum values were obtained on the extreme values, namely 0 and 100 % v/v (Fig. 7, C). This effect was correlated with the precision of the 3D printer and the nozzle diameter. Indeed, above an infill of 75 % v/v, a juxtaposition of the printed layers was observed, thereby reducing the total surface area of the 3D printed parts. Lastly, an inverse relationship was found for the surface/volume ratio. Indeed, higher S/V values were correlated with lower infill percentages.

However, for all these different relationships no impact of the layer thickness was observed. P-values of the parameters involved for the analysis of the surface, total weight, volume and surface to volume ratio are shown in Table 4.

From Table 4, it can be observed that the infill represents the parameter having the most important statistical impact on the surface, total weight, volume and surface/volume ratio with a $p < 0.05$. On the other hand, it can be observed that the different factors involving the layer thickness (B, AB and B^2) led to a p value higher than 0.05, indicating a low significant impact. In addition, there was no significant synergistic effect with the combination of the infill and the layer thickness ($p > 0.05$ for AB). Except for factor involving the layer thickness, F-values were largely greater than 1, indicating the models terms were significant (Annexes – Table S1). The predicted R^2 were in reasonable agreement with their adjusted R^2 with differences lower than 0.2. The adequate precision that is described as a signal-to-noise ratio of the different models was larger than 4 indicating adequate model discrimination (Table S1). Nevertheless, it is important to specify that the information obtained for the surface, the volume and their ratios were obtained after the analysis of the.gcode file transformed into a.stl file. Indeed, the quality of the.stl file supplied to the Meshmixer® program might not be precise enough to allow a discrimination between the different layer thickness. On the other hand, the total weight was evaluated after the printing of the different runs, which took into account the precision of the 3D printer.

In order to get an in-depth understanding of the impact of the layer thickness on the total weight, another figure was used based of each setting of the layer thickness. The data were represented as a one factor graph (Fig. 8), presenting the results of the infill (%) on the total weight (mg) of the 3D printed implants. Each graph is a representation of the response for each studied layer thickness (100, 200 and 300 μm).

As it can be seen in Fig. 8, it could be observed that the impact of the layer thickness was not homogeneous for the different studied values. Indeed, Fig. 8A showed the results obtained for printed parts with a layer thickness of 100 μm, representing the parameter with the fewest values

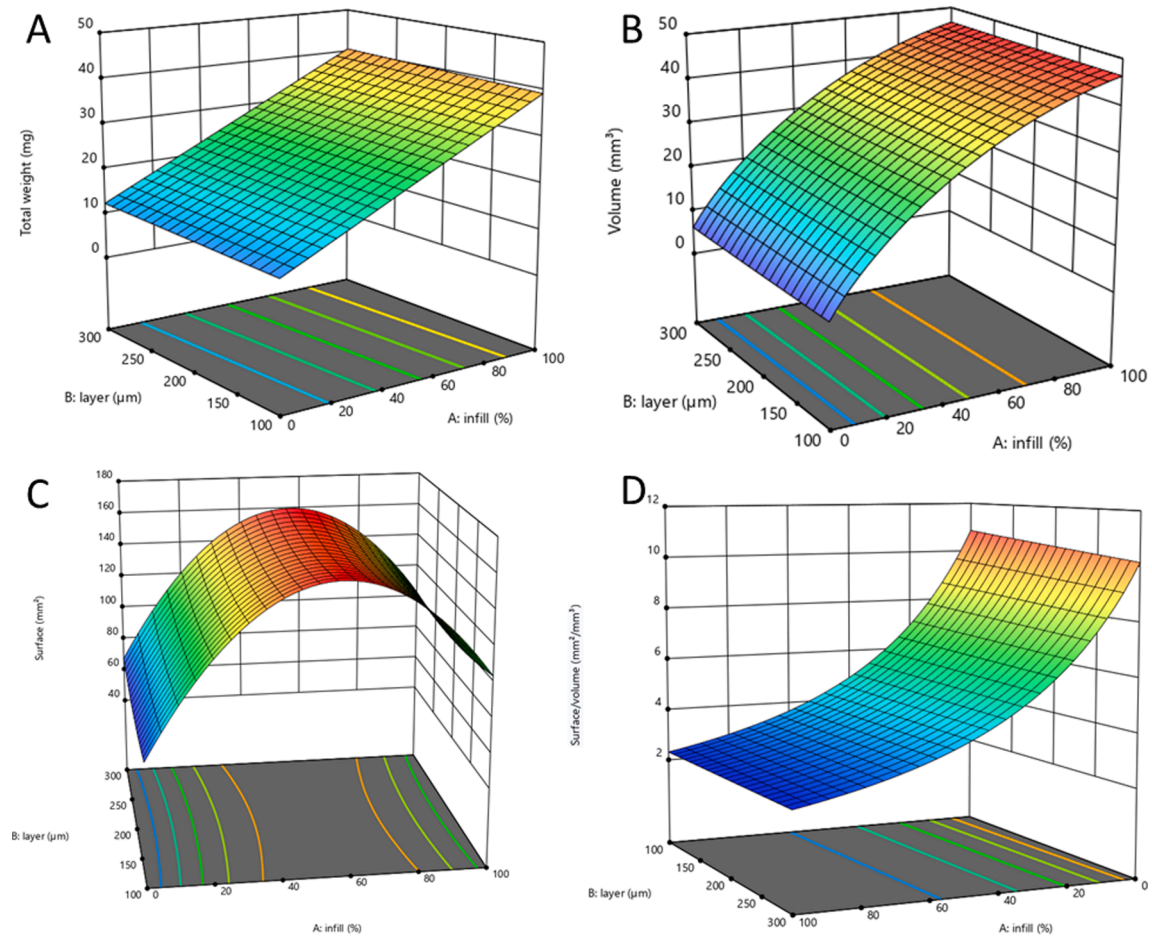

Fig. 7. Response surface models corresponding to the A) total weight, B) Volume, C) Surface and D) Surface/Volume ratio based on the infill (%) and layer thickness (µm).

Table 4
p-values of the infill (A) and the layer thickness (B) on the surface, total weight, volume and surface to volume ratio.

	p-values						R^2
	Model	**A - Infill**	**B - Layer**	**AB**	**A^2**	**B^2**	
Surface	< 0.0001	0.0001	0.892	0.854	< 0.0001	0.454	0.931
Total weight	< 0.0001	< 0.0001	0.579	–	–	–	0.903
Volume	< 0.0001	< 0.0001	0.585	0.932	< 0.0001	0.858	0.999
SV	< 0.0001	< 0.0001	0.425	–	–	–	0.9832

included within the IC95. In contrast, the results obtained with 200 and 300 µm (Fig. 8B and 8C) both showed 6 and 5 results within the IC95, respectively. These differences may be explained by the lack of adaptability of the printing parameters for each layer thickness studied.

Moreover, *Zhang et al.* also observed that the layer height did not had a significant effect on the weight of printed tablets. Indeed, three different layer thickness were studied: 0.05, 0.1 and 0.15 mm. No significant effect was observed on the weight based on a p-value of 0.9892 (>0.05). They suggested that the layer thickness might change the details of the printed tablet but not the overall design or the macro structure of the tablets (Zhang et al., 2020).

Indeed, FDM parameters such as the printing temperature, nozzle diameter, and printing speed can be identified as critical process parameters which have an influence on the final 3D printed shape (Zhang et al., 2020). However, in this study, a general 3D printing parameter was used for all the runs, namely a single printing temperature and identical printing speed. The printing quality of the layer thicknesses could have been improved by studying other factors such as different printing temperatures, printing speed or even nozzles with different diameters.

Indeed, this type of effect on the properties of the final 3D printed shape has already been highlighted by *Carlier et al.* where a morphological analysis by SEM was investigated on 3D printed parts. In their study, they investigated 3 printing temperatures (155, 173 and 190 °C), 3 thicknesses of layer (0.1, 0.2 and 0.3 mm) and 3 deposition speeds (1, 88 and 175 mm/s), all the experiments were done with a printer head equipped with a nozzle of 0.4 mm diameter. The results obtained showed different results in terms of printing quality. A lower resolution for parts printed with a layer thickness of 100 µm was observed. One of the explanations put forward was an extended contact of the printer head when the layer was set at 100 µm (Carlier et al., 2019). In their case, a higher morphological resolution was observed for parts printed with a layer set at 200 and 300 µm.

After this comparison, an *in vitro* dissolution test was performed. All the 3D printed dosage forms (Table 3) were placed in transparent vials and filled with 1.5 ml of dissolution medium. The test was carried out

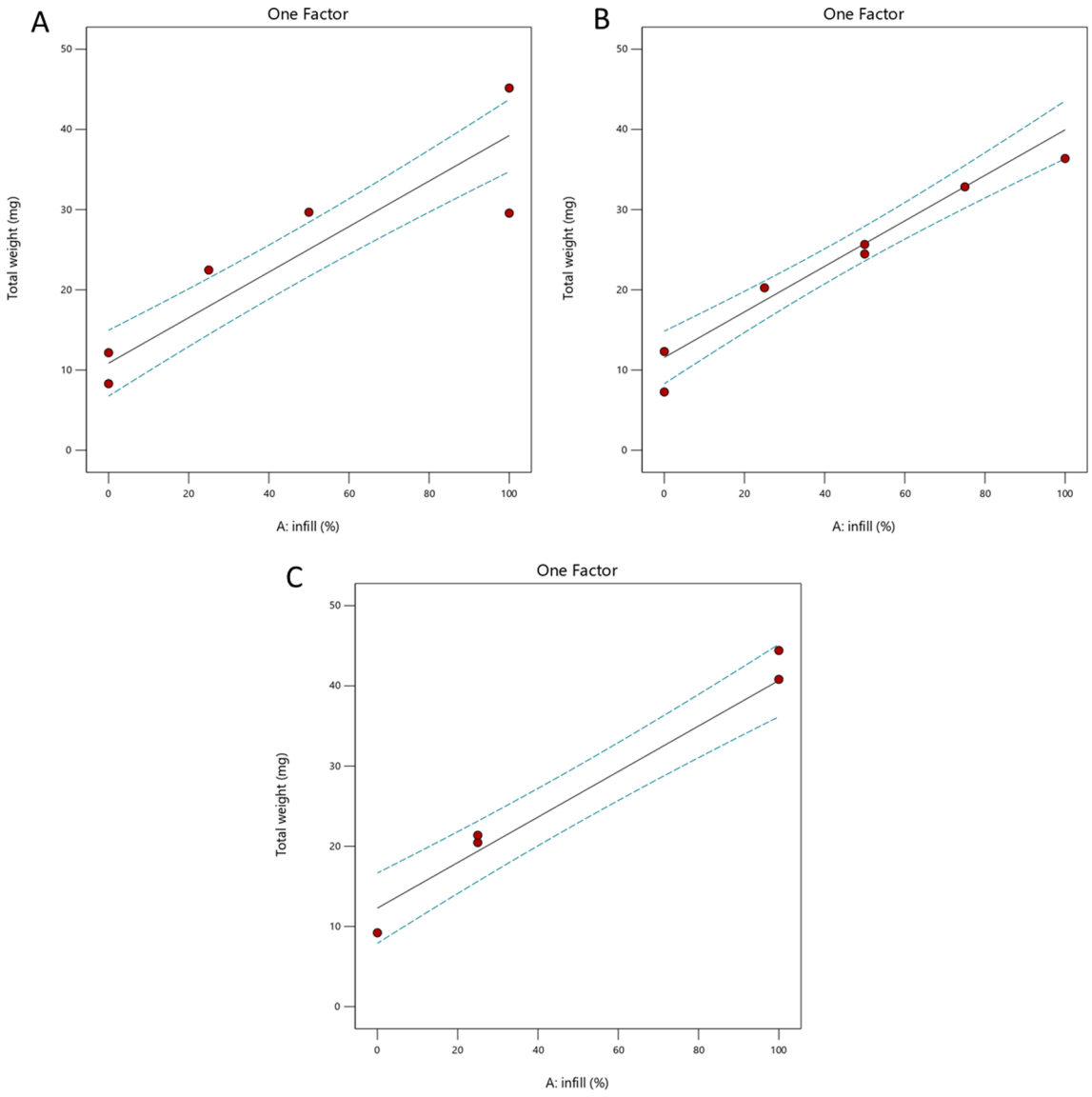

Fig. 8. One factor graph representing the linear effect of the infill (%) on the total weight (mg) for runs printed with A) 100 μm, B) 200 μm and C) 300 μm layer thickness. The 95 % confidence interval (IC95) is represented as dotted blue line. (For interpretation of the references to colour in this figure legend, the reader is referred to the web version of this article.)

over 28 days with 8 sampling spread over the duration of the dissolution test. During each sampling, the dissolution medium was entirely withdrawn and replaced by fresh one. After each sampling, the amount of PP that was released from the dosage forms was quantified by HPLC. The amount of drug released (μg) and cumulative drug released over time (μg) were analyzed with Design Expert® through a randomized response surface model (Fig. 9). An ANOVA was performed to evaluate if the models were significant ($p < 0.05$). The results presented in Fig. 9 represent the comparison of the impact between the infill and the layer thickness on the quantity of PP released after 1 day and after 28 days. A quadratic model was applied on the obtained results.

From day 1, it could be observed that a maximum of PP was released for infill values ranging between 50 and 75 % v/v (Fig. 9, A). This information can be correlated to the similar pattern observed with the graph representing the surface area in Fig. 7C. Indeed, the surface area was maximum for the corresponding infill values. In addition, the amount of PP released from implants with an infill of 0 % v/v were lower than those obtained from the monoliths. Moreover, the cumulative amount of PP released over 28 days (Fig. 9, B) was also correlated to the surface area of the printed dosage forms.

A GPC analysis was performed after 1 month of *in vitro* dissolution test on 3D printed dosage forms prepared with a layer thickness of 200 μm and 5 different infill percentages (0, 25, 50, 75 and 100 % v/v). Starting from a M_w of 220,000 ± 7300 g/mol and a dispersity (*D*) of 2.2 ± 0.1, a homogeneous polymer degradation was observed for the different studied infill percentages. Indeed, a homogeneous degradation of 25 % the M_w was observed after 1 month of dissolution test, corresponding to an average M_w of 165,000 ± 6,000 g/mol and a *D* of 2.4 ± 0.2. Based on these results, a modification of the infill did not increase the degradation rate of the polymer.

However, very different values were also obtained for implants printed with an infill of 100% v/v and a layer thickness of 100 μm. These discrepancies were in accordance with the results observed in Fig. 8A. Indeed, both graphs presented in Fig. 9 showed equivalent results in terms of drugs released for the parts printed with a layer thickness of 200 and 300 μm. The values obtained for the parts printed with a thickness of 100 μm need to be correlated to the lack of precision and the divergence coming from the critical process parameters highlighted above.

As it has just been described, the largest amount of PP was released with the parameters allowing the highest values of surface area. From

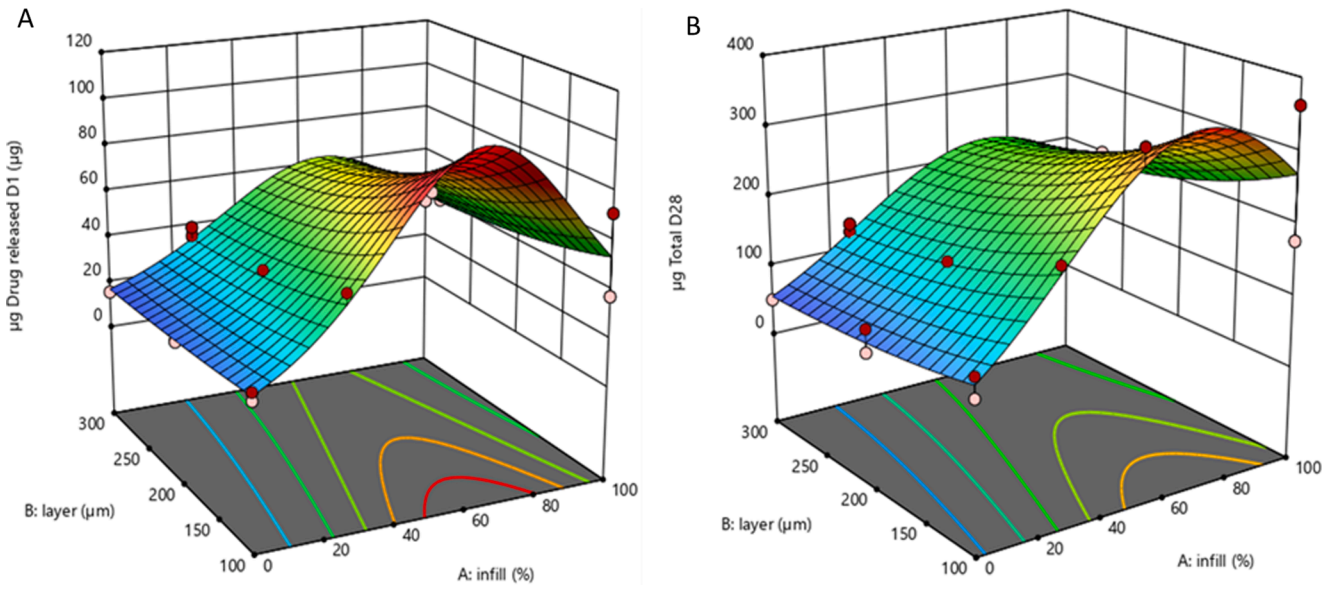

Fig. 9. Response surface models of A) Drug released (µg) at Day 1 and B) Cumulative drug released (µg) at Day 28 based on the layer thickness (µm) and the infill (%).

this point, a polynomial equation was determined for each sampling point. These polynomial equations allowed an estimation of the cumulative amount of PP as a function of the infill percentage and the layer thickness used as input parameters. These equations could be resumed as follow:.

$$Total\ \ drug\ \ release_n\ (\mu g) = A_n + B_n\boldsymbol{X} + C_n\boldsymbol{Y}\ + D_n\boldsymbol{XY}\ + E_n\boldsymbol{X^2} + F_n\boldsymbol{Y^2} \quad (1)$$

where "X" and "Y" are respectively the infill (%) and the layer thickness (µm), "*n*" corresponds to the sampling point and "*A to F*" are constant determined for each sampling point.

In order to verify the values obtained as well as the equations, input parameters were re-tested. Indeed, three values of infill were tested: 0, 60 and 100 % v/v. The values of 0 and 100 % v/v having already been observed, these points were re-tested to evaluate the validity of the model. The third infill value tested was 60% v/v, evaluated to be a maximum in terms of the amount of PP released and also presented as a point that was not tested among the 18 runs of the DoE. At the same time, two layer thickness were tested. The first part was carried out on the thickness which provided the highest number values within the IC95, corresponding to a layer thickness of 200 µm. In order to evaluate the limits of the prediction system, other conditions leading to failure were tested. Indeed, it has been observed that the results obtained with the implants printed with a layer thickness of 100 µm were not reproducible due to critical process parameters. Then, it was decided to reprint dosage forms with a layer thickness of 100 µm with the same infill as that tested for the 200 µm layer height: 0, 60 and 100 % v/v of infill. The new runs were printed in duplicate using the same printing parameters.

The mean weight of the 3D printed dosage forms were evaluated (Fig. 11). Then, an *in vitro* dissolution test was carried out on these new dosage forms. The dissolution parameters were kept identical to the above DoE. In parallel to the experimental results obtained via the *in vitro* dissolution test, Equation (1) was used to calculate the theoretical amount of PP released within a 95% confidence interval (Fig. 10).

From the experimental results obtained for the dosage forms printed with a thickness of 200 µm (Fig. 10, A-C) different amount of PP were released starting from day 1. Indeed, dosage forms printed with an infill of 0 % v/v released 16.3 ± 0.7 µg of PP, followed by the infill of 100 % v/v with 44.5 ± 3.5 µg and the highest amount of PP released from day 1 was obtained with the 60 % v/v infill, 73.1 ± 3.2 µg of PP. The trend was maintained throughout the duration of the *in vitro* dissolution test.

Indeed, after 28 days, the dosage forms printed with an infill of 0 % v/v which released 63.7 ± 6.0 µg, followed by the implants with an infill of 100 % v/v with 208.3 ± 6.3 µg of PP and finally, the implants printed with an infill of 60 % v/v with 262.6 ± 52.9 µg of released PP. On the other hand, different results were observed for dosage forms printed with a layer thickness of 100 µm, Fig. 10, D-F. Even if results obtained from infill of 0 v/v and 60 % v/v were in accordance with those obtained with 200 µm, disparities were observed with dosage forms printed with a 100 % v/v of infill (Fig. 10F). Indeed, infill of 60 % v/v released higher amount of PP from day 1 to day 28 with 97.8 ± 2.6 to 363.2 ± 5.6 µg of PP released (Fig. 10E). These results were higher than those obtained with an infill of 0 % v/v corresponding to 25.3 ± 1.3 to 93.0 ± 4.6 µg of PP released (Fig. 10D). It can be observed that the experimental results described for Fig. 10 (A-E), whatever was the infill used, fitted within the IC95 predicted by Equation (1) for each sampling point. Indeed, even though the standard deviation obtained for the experimental dosage forms with an infill of 60 % v/v showed a larger deviation, the results were within the IC95 (Fig. 10B).

However, the drug release obtained from the dosage forms printed with 100% v/v of infill and a layer of 100 µm (Fig. 10F) were outside the IC95 and the theoretical expected values. These results highlighted an issue of reproducibility as these parameters had already been tested during the DoE (Runs 1 and 9). Despite experimental values outside the expected ones from Fig. 10F, no significant statistical differences ($p > 0.05$) were observed from the student *t*-test.

These results clearly indicated the interaction between the infill and parameters such as the surface area but also the total volume of the printed dosage forms which are impacting the amount of drug released. In addition, the difference in quantity released as a function of the filling parameter could vary by a factor of 4 from the start of the dissolution test up to 1 month later.

Comparatively, *Dos Santos et al.* prepared dexamethasone-loaded polycaprolactone filaments and studied the impact of different parameters on the release of the drug from 3D printed dosage forms. Among the parameters studied, the effect of mannitol as a channeling agent, two different infill percentages (50 and 100 % v/v), as well as two percentage of drugs (5 and 10 % w/w), were investigated. They also observed that the infill percentage was the main factor responsible for customizing the release of the drug from the solid form (dos Santos et al.,

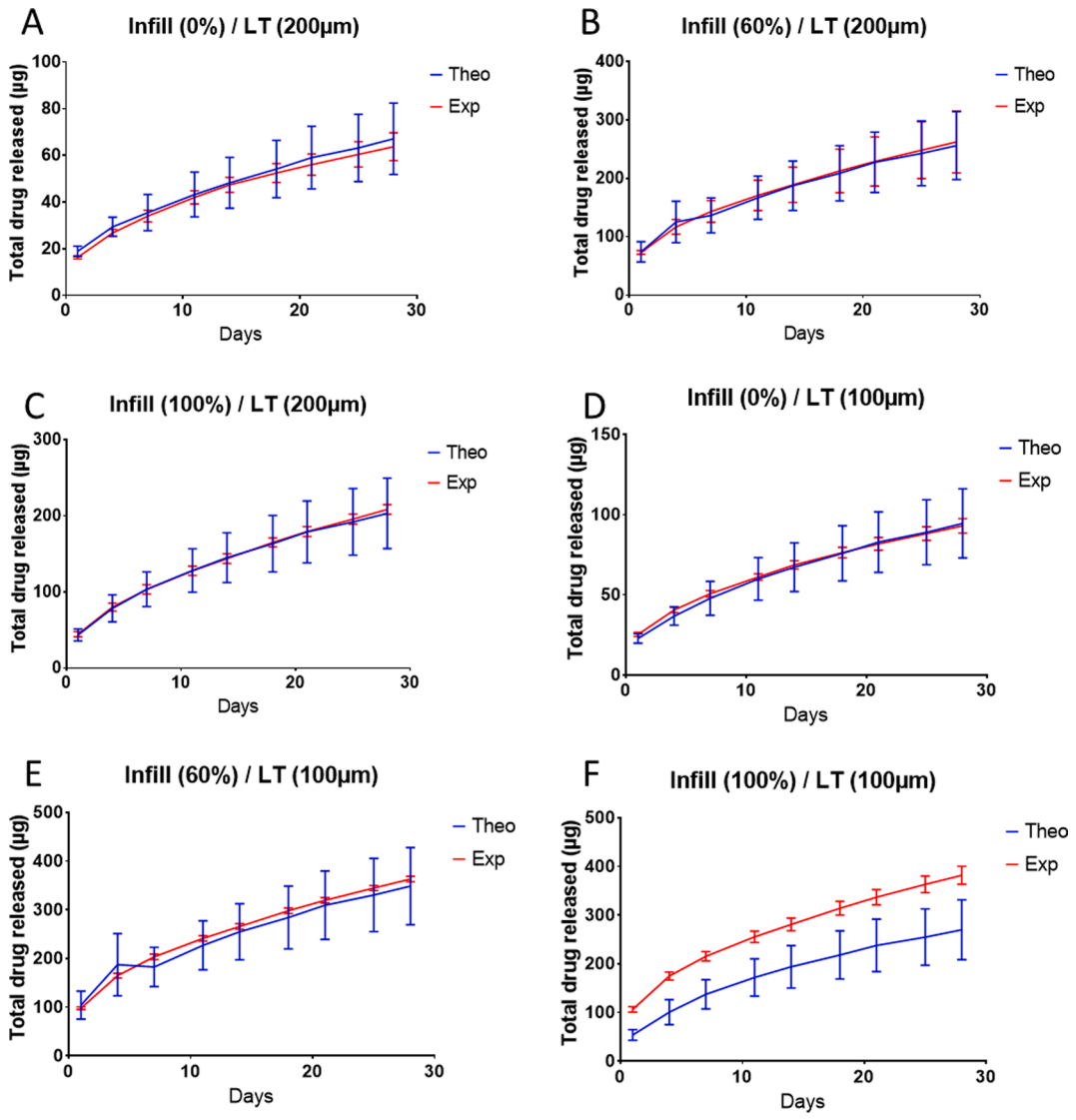

Fig. 10. Cumulative PP release over time A-C) Infill (0 % – 60 % – 100 %) / LT (200 µm) and D-F) Infill (0 % – 60 % – 100 %) / LT (100 µm). Theoretical values within IC95 are presented in blue and the experimental values (Mean ± SD, n = 2) are presented in red. LT corresponding to the layer thickness. (For interpretation of the references to colour in this figure legend, the reader is referred to the web version of this article.)

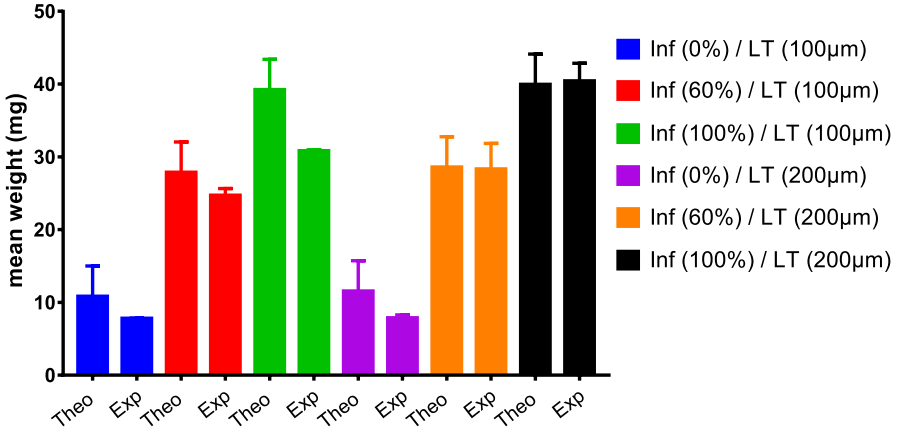

Fig. 11. Comparison of theoretical within an IC95 and experimental (mean ± SD, n = 2) mean weight (mg) of 3D printed dosage forms with different infill (0% – 60% – 100%) and layer thickness (100 µm and 200 µm).

2021).

In order to distinguish the limitations of the prediction system, a specific attention has also been pointed to the prediction of the mass of the printed dosage forms (Fig. 11). This prediction had the advantage of allowing a direct control of the process, which can be carried out just after the printing step. Simultaneously, an equation was obtained from the results presented on Fig. 7A, presenting the total weight resulting from the layer thickness and infill. The total weight prediction system was based on a linear model described by Equation (2):.

$$Total\ weight\ (mg) = A + BX + CY \quad (2)$$

where "X" and "Y" are respectively the infill (%) and the layer thickness (μm) and "*A to C*" are constants.

The theoretical mass of 3D printed dosage forms was calculated within an IC95 and compared to the experimental values. From these results, all the experimental values were found in the IC95 interval of the predicted theoretical values. However, only one value was found outside of those predicted. These dosage forms were printed with a maximal infill percentage and a layer thickness of 100 μm. Indeed, the predicted theoretical value was 39.2 ± 4.2 (mg) and the experimental value obtained was 30.8 ± 0.1 (mg). This difference between the experimental and theoretical predicted value could be correlated with the results of the predictions obtained from Fig. 10F. The experimental values were outside the expected amount of PP released during the predicted time. The information obtained by measuring the weight in comparison with the expected theoretical value allowed carrying out a first quality control step before starting an *in vitro* dissolution test. However, even if the results of this quality control seems interesting, no significant statistical differences ($p > 0.05$) were observed between the expected and theoretical implant mass.

This study presented the versatility of 3D printing as manufacturing process in personalization of dosage form without adaptation of the formulation. Indeed, 3D printing techniques were already used to produce different 3D geometric shapes from an unique formulation showing different release profiles (Manini et al., 2021; Goyanes et al., 2015). Beyond this, a specific parameter to 3D printing such as the infill percentage demonstrated its capability to modify the release profile of a dosage form without modifying its overall geometry.

Despite the results observed in this work illustrating the direct impact of the surface area on the release of PP over time, other parameters must also be considered and studied. Indeed, the discrepancies of results obtained by modulating the layer thickness required further investigations especially the critical process parameters and their impact on the final printed dosage form.

Moreover, comparative studies with other 3D printers should be carried out to corroborate the obtained results. Indeed, *Pires et al.* have shown that the use of different printers has a significant impact on the quality of printed products. Significant variations were observed in terms of masses, mechanical structures as well as different results in terms of material deposition. In addition, some variations were greater with one printer than another. Indeed, they observed greater variations in tablet masses with the Makerbot Replicator 2X® rather than using the Voolt3D Gi3® printer. As a result, a validation process will be mandatory specifically for each 3D printer (Pires et al., 2020).

Nevertheless, *in vivo* studies are also mandatory to confirm the above observations. Large disparities could be observed from *in vitro* to *in vivo* results (Bhardwaj and Burgess, 2010; Darville et al., 2014; Li et al., 2013; Li et al., 2013). In addition, it has already been mention for long-acting dosage forms that there is actually no *in vitro* particle-oriented dissolution test, allowing the inclusion of the complexity observed *in vivo* (Bhardwaj and Burgess, 2010; Darville et al., 2014).

3.3. Part II - comparison between predicted and experimental values of drug release from complex 3D printed dosage forms.

In this second part, a study was carried out for the preparation of 3D printed dosage forms based on two different formulations. For this purpose, a 3D printer supplied by multiple heads was selected. From this technology, different materials or formulations can be printed leading to a multi-material 3D printed dosage form.

In the literature, this technology has already been investigated for the preparation of "polypill" printed by FDM (Pereira et al., 2019). This technology is attractive to separate different drugs that cannot be formulated together due to incompatibilities or to obtain different release profiles.

Despite the results presented in Part I showing the effect of the infill on the amount of PP released, the different release profiles remained specific to a given geometric shape. Indeed, only the infill and the layer thickness were modified in Part I. Even if the release of PP over time was correlated to the variation of surface area and volume generated by a modification of the infill, the design of the dosage form was limited. When the infill was modified, the parameter influenced the surface area, but it also had a simultaneous impact on the volume. It was not possible to change the volume of the dosage form without affecting the surface area.

The aim of this last part was to go further in the realization of a release profile that could be depicted from the surface and the volume of a dosage form. Whatever the design of the dosage form used, the goal was to get rid of a defined implant geometry.

3.3.1. Design of experiments

The aim was to determine the amount of PP released over time solely based on a measurement of surface area and volume. This technique will no longer be limited to a single implant geometry or infill percentage.

A DoE was used to solve this issue. Starting from the postulate that the release was dependent of the surface area, the volume and their ratio (S/V), the work was carried out on two inputs parameters: the volume and the S/V ratio. Among these parameters, 3 discrete values were studied for each parameter. In order to study different volumes and surfaces, the initial design was a cylinder (Fig. 12).

Indeed, by modifying the height and the diameter of the cylinder, the cylindrical design allowed the modification of the volume of the printed form while preserving the surface area (Fig. 12 – Table 5). After generating the various.stl files, the surface area and volume of the 3D dosage forms were calculated using Meshmixer® program.

By modulating the diameter and the height of the 3D printed dosage forms, it was possible to obtain cylinders having different volumes while keeping the same surface area. Indeed, by comparing the volume and surface area of V_80/SV_4 and V_60/SV_6, both designs had a surface area of 360 mm^2 but different volumes and loadings of PP. By going through an *in vitro* dissolution test, it was possible to discriminate the impact of the surface area and volume on the amount of PP released over time. Both formulations (Table 1), based on PLA-EVA-PP and PLA-PCLLA-PP were investigated in this study. The same DoE based on 16 runs was applied for both formulations (Table 6).

For both formulations, the 3D printed dosage forms were printed using the same printing parameters than those described in Part I. The layer thickness set for all the 3D dosage forms was 200 μm and a first layer of 100 μm was applied for cylinder with an impair layer height.

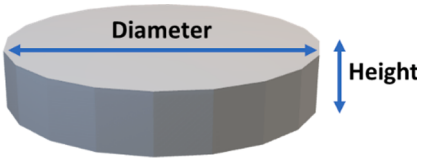

Fig. 12. 3D design of the cylindrical shape used for the design of experiments.

Table 5
Dimensions used to prepare tablets with specific volume and S/V ratios.

Name	Volume (mm^3)	S/V (mm^2/mm^3)	Diameter (mm)	Height (mm)	Surface (mm^2)
V_40/SV_2	40	2	5.8	1.5	80
V_40/SV_4	40	4	9.6	0.6	160
V_40/SV_6	40	6	12	0.3	240
V_60/SV_2	60	2	7.5	1.4	120
V_60/SV_4	60	4	11.8	0.5	240
V_60/SV_6	60	6	14.8	0.3	360
V_80/SV_2	80	2	8.9	1.3	160
V_80/SV_4	80	4	13.8	0.5	360
V_80/SV_6	80	6	17.1	0.3	480

Table 6
Design of Experiments based on 2 inputs parameters: Volume (mm^3) and the surface to volume ratio (S/V) (mm^2/mm^3).

Runs	Factor 1 vol (mm^3)	Factor 2 S/V (mm^2/mm^3)
1	80	4
2	60	4
3	80	6
4	60	6
5	60	6
6	60	4
7	60	2
8	40	2
9	40	6
10	40	4
11	60	4
12	40	2
13	80	2
14	40	2
15	60	4
16	80	4

After printing, the dosage forms were weighed and placed in transparent vials filled with 1.5 ml of dissolution medium. The *in vitro* dissolution test was carried out under the same conditions than that described in Part I, with the same sampling parameters. An ANOVA was performed to evaluate the impact of the input parameters on the surface, total weight and amount of PP released from 3D printed dosage forms. Randomized response surface models were investigated to discriminate the impact of the volume and S/V on the surface and weight of 3D printed tablets (Fig. 13).

The results presented in Fig. 13 showed the surface area values obtained via the Meshmixer® program (Fig. 13, Left) and the results after weighing the printed shapes (Fig. 13, right). From the ANOVA, a two-factor interaction model (2FI) model was applied for the surface area and a linear model was applied for the total weight analysis of the 3D dosage forms. The R^2 and p-values of these models are presented in Table 7.

The response surface model (Fig. 13, left) showed a clear representation of 3D printed dosage forms having equivalent surfaces with different volumes. On the other hand, the total weight of the printed dosage forms was linearly correlated to their volume (Fig. 13, right). From the different geometry studied, a variety of 3D shapes with surfaces area ranging from 80 to 360 mm^2 and weights from 40 to 90 mg were studied, respectively. The values presented in Fig. 13 concerning the PLA-PCLLA-PP formulation were equivalent to the values obtained for the PLA-EVA-PP formulation.

The p-values presented in Table 7 showed that the different terms used: A, B and AB were significant ($p > 0.05$) as well as the 2FI and linear models applied. The results of PP released from the *in vitro* dissolution test after 1 day, as well as cumulative release after 28 days were studied according to a response surface model (Fig. 14).

From the ANOVA results, differences lower than 0.2 were observed between the adjusted R^2 and predicted R^2 (Table S2). In addition, the adequate precision was also largely greater than 4 for both formulations. A 2FI model was applied on the values obtained after 1 day of *in vitro* dissolution test for the PLA-EVA-PP formulation (Fig. 14, A) and a linear model for the PLA-PCLLA-PP formulation (Fig. 14, C). The different input parameters were significant ($p < 0.05$), F-values $\gg 1$ for each model (Table S2), the R^2 of the model was 0.9105 for PLA-EVA-PP formulation and 0.9566 for the PLA-PCLLA-PP formulation. The release of PP after 1 day could be correlated with the surface area of the 3D printed dosage forms, whatever the formulation used (Fig. 14, A and C). The smallest and largest amounts of PP were released respectively for the smallest and largest studied surfaces. The smallest amount of PP was released from the printed dosage form V_40/SV_2 having a surface area of 80 mm^2 and the highest amount of PP was released from the dosage form V_80/SV_6 with a surface area of 480 mm^2. However, even if the 3D dosage forms printed with these parameters had opposite surface value, they also presented clear differences in terms of volume. Indeed, the smallest amount of PP was released from dosage forms with a volume of 40 mm^3 and the largest amount of PP was released from dosage forms with a volume of 80 mm^3. Despite this fact, 3D dosage forms can be classified based on their S/V ratio. Indeed, S/V ratios equal to 6 released more PP than the S/V of 4, which also released more PP than the S/V ratios equal to 2. These results agreed regardless of the volume

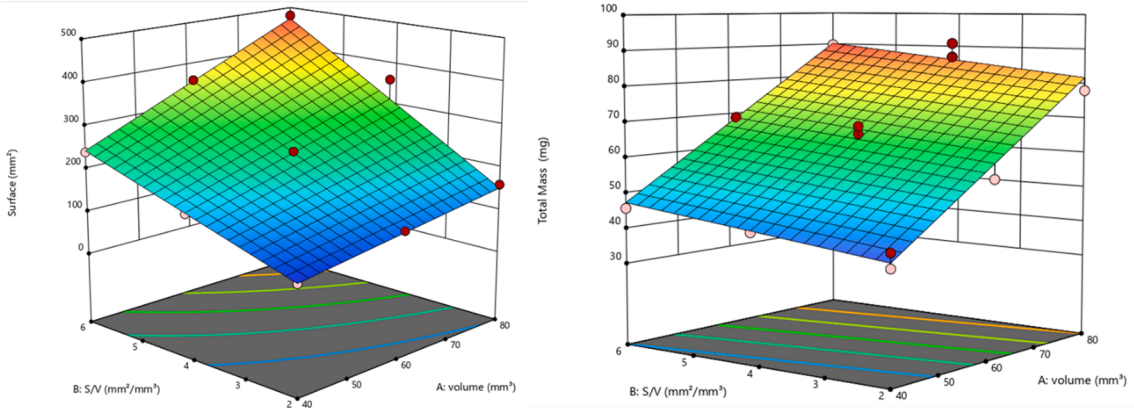

Fig. 13. Response surface analysis of the volume and S/V on the surface (left) and total mass (right) based on the PLA-PCLLA-PP formulation.

Table 7
p-values and R^2 obtained from the ANOVA. With "A" corresponding to the volume and "B" the S/V ratio.

Formulations		p-values				R^2
		Models	A - Volume	B - S/V	AB	
PLA-EVA-PP	Surface	<0.0001	<0.0001	<0.0001	<0.0001	0.99
	Total weight	<0.0001	<0.0001	0.0453	x	0.9276
PLA-PCLLA-PP	Surface	<0.0001	<0.0001	<0.0001	<0.0001	0.991
	Total weight	<0.0001	<0.0001	0.0006	x	0.979

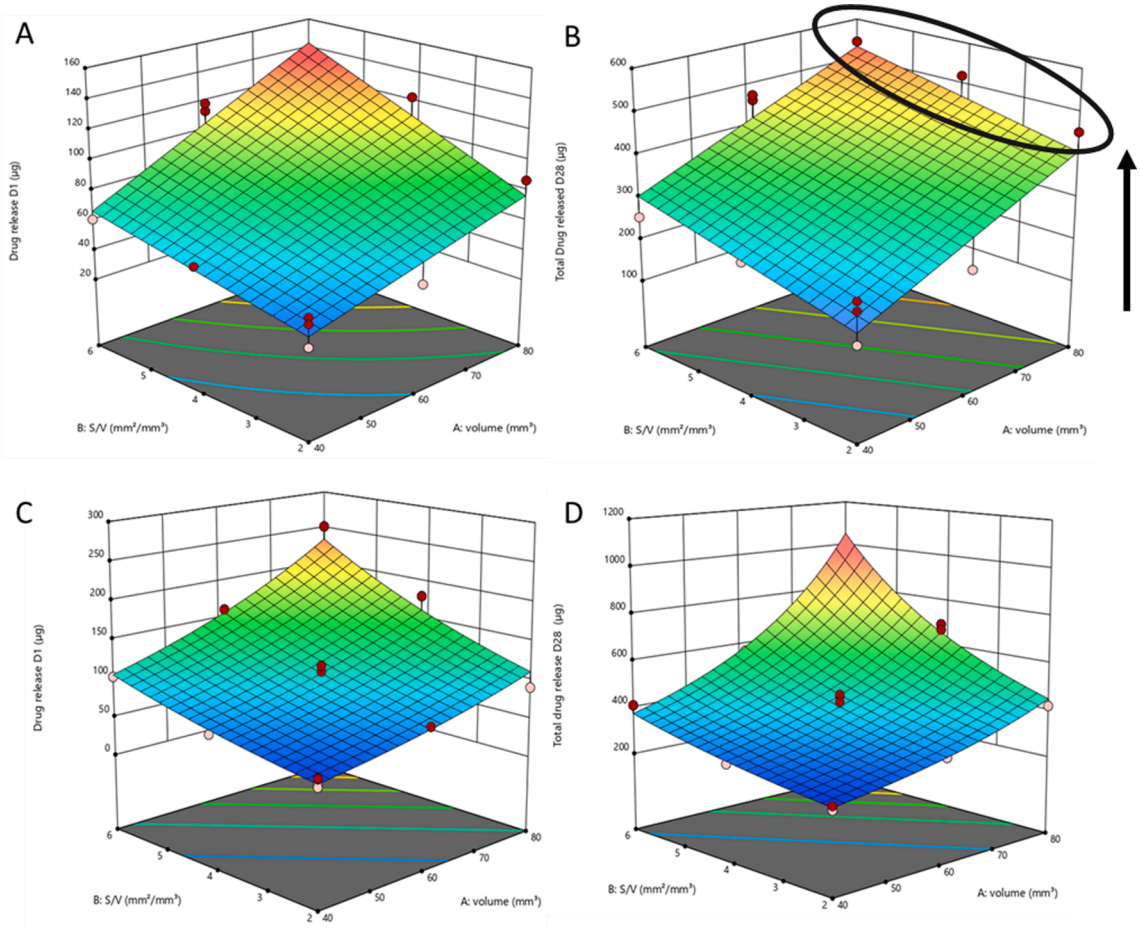

Fig. 14. Response surface model of the drug release after 1 day for PLA-EVA-PP (A) and PLA-PCLLA-PP (C) and the cumulative drug release after 28 days respectively for PLA-EVA-PP (B) and PLA-PCLLA-PP (D).

studied and independently of the formulation.

After 28 days, results were presented as response surface models in Fig. 14 (B and D). From the ANOVA, a linear model was applied on the results from both formulations. Models and terms were significant with p-values < 0.05 and F-values greater than 1, the R^2 for the PLA-PCLLA-PP formulation was 0.9694 and 0.8369 for the PLA-EVA-PP formulation. After 28 days of dissolution test, cumulative drug release based on V_40/SV_2 and V_80/SV_6 showed the largest differences. Indeed, as observed after 1 day, at the end of the dissolution test, both parameters showed respectively the lowest and the largest amount of PP released over 1 month independently of the formulation. Moreover, for each studied volume, the impact of the S/V ratio was kept similar, higher S/V ratio were correlated to higher amount of PP released.

However, despite all these similarities between the formulations, disparities were also highlighted. Indeed, these disparities concerned the amounts of PP released depending on the formulation. Larger amounts of PP were released after the 1st day of dissolution test for the dosage forms printed with the PLA-PCLLA-PP formulation. Taking the extreme values from V_40/SV_2 and V_80/SV_6, 33 to 135 µg of PP were released for the PLA-EVA-PP formulation against a range of 45 to 250 µg of PP released from the PLA-PCLLA-PP formulation. After 1 month, a range of 150 to 540 µg of PP were released from the PLA-EVA-PP formulation against a scope ranging from 200 to 970 µg from the PLA-PCLLA-PP formulation. One of the explanations might come from the composition of these formulations. These formulations contained 18 % EVA or 22.5 % PCLLA, both polymers having different drug release capacities. Indeed, EVA being a non-bioresorbable polymer, the release of PP will take place according to diffusion phenomena, while PCLLA as a bioresorbable polymer released PP from erosion and/or degradation.

This hypothesis could be correlated with the results observed in Fig. 14, B. Even if there was a difference between the quantities released as a function of the S/V, the values were less disparate for the PLA-EVA-PP formulation (Fig. 14B, black circle) than for the PLA-PCLLA-PP formulation. By comparing the cumulative quantity of PP obtained after 28 days for the forms V_80/SV_2 and V_80/SV_6, respectively 454 and 543 µg of PP were released from the PLA-EVA-PP formulation

against 471 and 972 µg for the PLA-PCLLA-PP formulation. There was only an increase of 20 % w/w of PP released for the PLA-EVA-PP formulation against more than 100 % w/w of increase for the PCLLA-based formulation in the quantity of PP released by modulating the S/V ratio.

From these results, an equation was determined allowing the calculation of the amount of PP released as a function of the volume and S/V parameters for each sampling time:.

$$Total\ \ drug\ \ release\ \ (\mu g) = A_n + B_n\boldsymbol{X} + C_n\boldsymbol{Y}\ \ (+ D_n\boldsymbol{XY}) \quad (3)$$

where "n" represents the sampling time, "X and Y" represent the volume and the S / V ratio respectively. The term "XY" was used when a 2FI model was investigated. The terms "A to D" were specific constants for each sampling point.

In order to evaluate the model represented in Equation (3), complex structures were created from both studied formulations. The initial form was determined to be a disk shown in Fig. 15, A. Both formulations, PLA-EVA-PP and PLA-PCLLA-PP could be simultaneously used to prepare the 3D printed dosage forms due to the double printer head of the Raise3D Pro2®. Two complex structures were studied. The first one was performed by separating the initial shape according to its diameter (Fig. 15, B). The second one was performed via two superimposed disks (Fig. 15, C). Following the preparation of the.gcode via the Ideamaker® program, the files were transformed into.stl using the Voxelizer® program. Meshmixer® was used to evaluate the surface, volume and ratios of the new structures. Then, both designs were printed at 150 °C, with a layer thickness of 0.2 mm and an infill of 60 % v/v.

Through the use of a multiple head 3D printer, it was possible to divide the initial disk into two half-disks, where each part corresponded to a formulation. Indeed, in Fig. 15 D&F, the PLA-EVA-PP formulation was used to print the right part and the PLA-PCLLA-PP formulation was used to print the left part. On the other hand, when the disc was separated into two superimposed disks, the PLA-EVA-PP formulation was below, and the PLA-PCLLA-PP formulation was above. The use of a printing temperature of 150 °C, as well as the various printing parameters used, allowed the obtention of an acceptable print quality (Fig. 15, F), compared to the.stl file (Fig. 15, B). However, despite different modifications of printing temperature, printing speed or even the cooling, the superimposed pieces did not show a total adhesion over the whole piece. This lack of adhesion between both formulations was visible at the edges of the printed part (Fig. 15, G). An *in vitro* dissolution test was performed on the 3D printed parts (Fig. 15, F & G). The test was carried out under the usual conditions and in duplicate.

Based on the DoE carried out on each formulation, the volume analysis, surface area of each dosage form, as well as the use of Equation (3), curves predicting the amount of PP released over time were calculated. Indeed, these curves represented the cumulative quantities of each formulation involved in the new forms, the double-half disks (Fig. 16) and the superimposed disks (Fig. 17). To obtain these predictions, the Meshmixer® program determined the surface and volume of these shapes.

The analysis of a half-disk determined a volume of 71 mm^3 and a surface of 321 mm^2 with a S/V ratio of 4.5 (Fig. 16). By using these values into Equation (3), a PP release from day one of 250 ± 19 µg were expected. The experimental results obtained for the first day were slightly lower than expected with 175 ± 18 µg of PP released. Over time, the difference between the predicted and experimental results was reduced to expect after 1 month, an experimental quantity of PP 980 ± 97 µg released against 1010 ± 80 µg predicted. From the student *t*-test, no significant differences ($p > 0.05$) were observed between the experimental and predicted results.

For the second design (Fig. 17), the surface and volume were calculated on disks with half the height of the original one. More specifically, the analysis was done on a disk measuring 14 mm in diameter and 0.6 mm in height, instead of 1.2 mm in height. Indeed, as both disks were not fully adherent to each other, the dissolution medium can penetrate more easily within the structure. Each smaller disk was identified with a volume of 74 mm^3 and a surface of 455 mm^2, corresponding to a S/V of 6.2. As it can be observed, these values were clearly higher than those obtained with the "half-disks".

After the 1st day of dissolution test, the amount of PP released was close to the predicted amount with 270 ± 28 µg of PP released and 339 ± 37 µg predicted. The experimental results were close to the predicted one until 7 days. Then, the drug release from the printed designs was

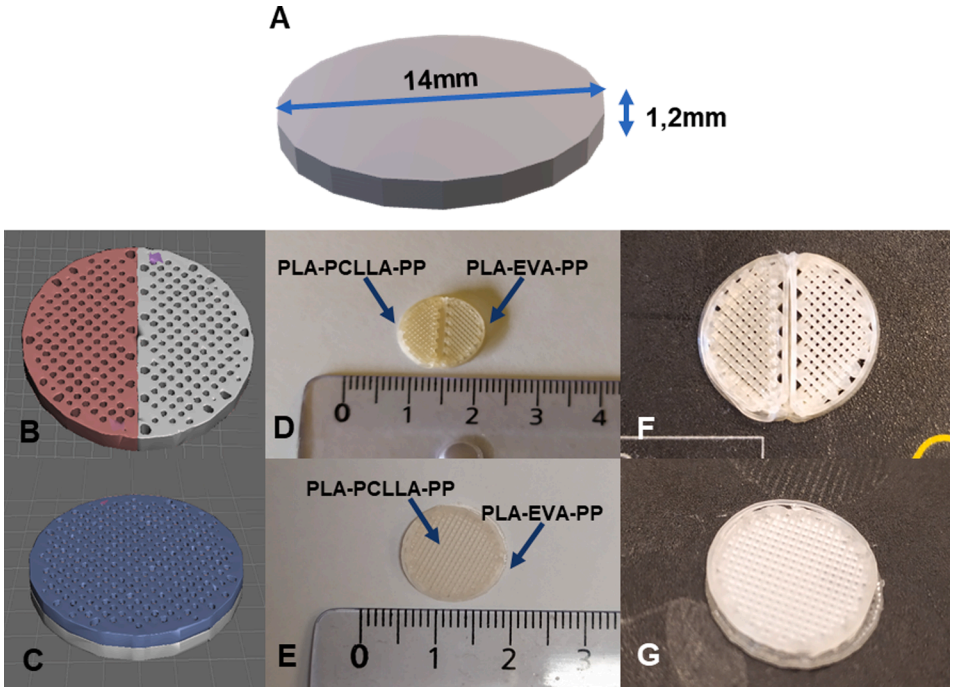

Fig. 15. A) 3D dimensions of the dosage form, B and C) Designs of dosage forms after slicing, D to G) 3D printed dosage forms based on PLA-EVA-PP and PLA-PCLLA-PP.

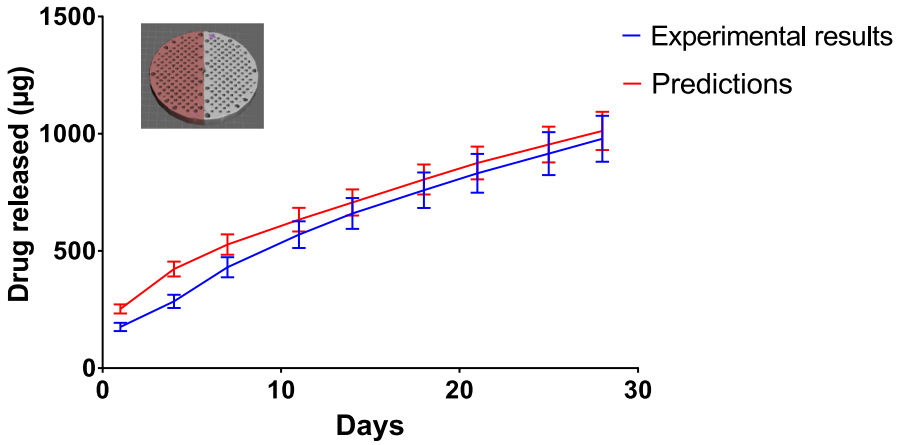

Fig. 16. Experimental (Mean ± SD, n = 2) and predictions (Mean within an IC95%) amount of PP released from the double half-disks.

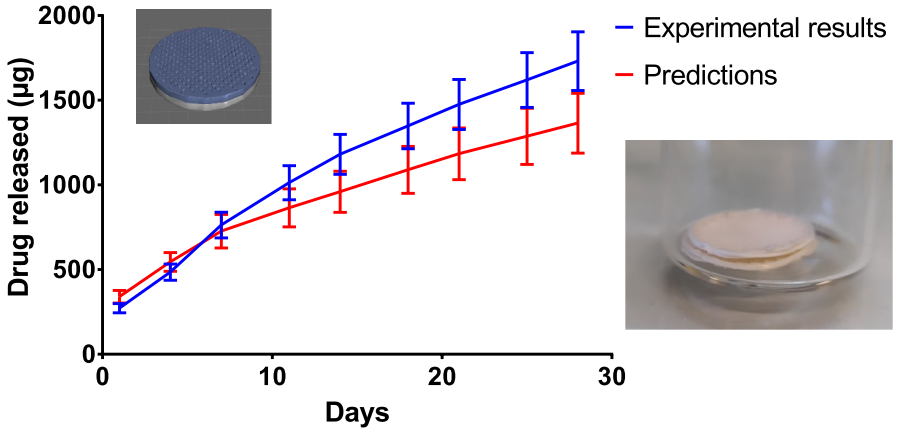

Fig. 17. Experimental (Mean ± SD, n = 2) and predictions (Mean within an IC95%) amount of PP released from the superimposed disks.

higher than predicted. After 28 days, 1,730 ± 170 µg of PP were released instead of 1,360 ± 176 µg, respectively. No significant statistical differences ($p > 0.05$) were observed between both profiles. However, an explanation for this difference may come from the poor adhesion at the intersection of both formulations. Indeed, even by predicting the amount of PP from two separate disks, the amount released was still higher. From one side, this adhesion problem might have an impact on the upper layers, reducing the adherence within each separate disk. Bonding issues are recurrent in FDM especially with multi-materials. The investigation and optimization of processing parameters such as different nozzle temperatures are often necessary (Lin et al., 2018). On the other side, further investigation should also be done regarding the *in vitro* dissolution tests. Indeed, there is currently a lack of standardization regarding the *in vitro* dissolution tests of implantable dosage forms as *in vivo* conditions are difficult to reproduce *in vitro*. Hydrogel-like environment is another technique that could be investigated. In this case, the release medium is replaced by an hydrogel, such as an agarose gel (Kožák et al., 2021). This type of environment has been suggested as a more realistic *in vitro* release model than the actual bulk fluid (Hoang Thi et al., 2010; Stewart et al., 2020).

Larger amounts of PP were released from the double disks than the "half-disks". This difference in quantity can be explained by the surface area and S/V ratio between both studied designs. In the case of the "superimposed disks", each disk had a surface area 30 % higher than the half-disks, as well as a greater S/V. However, it was shown during the DoE that these two parameters had a direct effect on the quantity of PP released, especially with equivalent volumes.

However, even though this work was done on two different formulations, they both contained equal proportions of PP. This type of study can be used as a starting point to carry out complex 3D forms comprising different drug-loaded formulations. It might be also interesting to compare the results obtained with this DoE with those obtained by other techniques able to predict the drug release of different dosage forms. More recently, artificial intelligence has been applied to predict the printability and drug release from FDM-based drug delivery systems (Elbadawi et al., 2020). *Muñiz Castro et al.,* applied machine learning over 900 formulations mined from the literature. By using this alternative approach, it is also possible to predict the drug dissolution profiles (Muñiz Castro et al., 2021).

In this study, additive manufacturing has shown its ability to prepare implantable dosage forms. However, the use of implants is not only limited to the treatment of schizophrenia as they may be used to prevent cancer recurrence (Hope et al., August 2021) or for the treatment of infections or inflammation (Lizambard et al., 2019). For instance, *Xu et al.*, have investigated 3D printing for the preparation of lidocaine-loaded bladder devices for the treatment of intravesical disease. The use of an implantable dosage form allowed a prolonged and localized release of lidocaine over 14 days (Xu et al., 2021). In another study, *Stewart et al.*, investigated poly(caprolactone)-based coated implants to sustain the delivery of hydrophilic drugs such as methylene blue or ibuprofen sodium. They highlighted the importance of such dosage forms, especially when the patient is facing a poor medication adherence. (Stewart et al., 2020).

In addition, this work also showed the importance of measurements such as the surface area and the volume on the amount of PP released. Even if 3D printing allows a lot of freedom, the realization of complex

shapes may nevertheless require adaptations and additional in-depth analysis. Indeed, even if both formulations were mainly composed with the same PLA and the same amount of PP, adhesion problems came out. This phenomenon highlighted that even if 3D printing remains an easily accessible technology, 3D printing of pharmaceutical dosage forms remains a challenge.

4. Conclusion

This proof of concept showed the possibility of 3D printing technology to be an adaptative solution to the needs of specific patients. FDM has already been widely studied for immediate release forms but it may also offer an adequate solution for the personalization of long-acting treatments. This work highlighted the interest of DoE as a tool and the determination of CQA such as the surface and the volume of 3D designs on the quantity of PP released over time. Indeed, in Part I, the use of the infill parameter could be clearly correlated to different release profile of PP and could be adapted for further personalized treatment. Without modifying the overall geometry of the 3D printed dosage form, the amount of PP release was modulated by a factor 4. Moreover, the theoretical results expected through the use of a prediction system were in agreement with the experimental values obtained during the *in vitro* dissolution test. However, differences were observed when the layer thickness was modified. A specific attention must be given to the modulation of the layer thickness which remained to critical process parameters which are specific for each 3D printer and formulations. The additional investigations carried out in Part II of this work put forward the realization of printed forms using multiple printer heads. Even if, additional studies need to be carried on such as *in vivo* studies, the methodology applied in this study can be used as a starting point on other drugs, formulations and 3D printers.

Declaration of Competing Interest

The authors declare that they have no known competing financial interests or personal relationships that could have appeared to influence the work reported in this paper.

Acknowledgements

Giuseppe Manini was supported by the Belgian Fund for Research training in Industry and Agriculture for its financial support (FRIA grant). S. Benali thanks the special supports by the European Community (FEDER) in the frame of LCFM-BIOMAT and Interreg France-Wallonie-Vlaanderen program, 3D4Med. J.M. Raquez is Maitre de Recherches from Belgiam FNRS agency.

Appendix A. Supplementary material

Supplementary data to this article can be found online at https://doi.org/10.1016/j.ijpharm.2022.121663.

References

Allaf, R.M., Albarahmieh, E., AlHamarneh, B.M., 2019. Solid-state compounding of immiscible PCL-PEO blend powders for molding processes. J. Mech. Behav. Biomed. Mater. 97 (February), 198–211. https://doi.org/10.1016/j.jmbbm.2019.05.023.

Awad, A., Yao, A., Trenfield, S.J., Goyanes, A., Gaisford, S., Basit, A.W., 2020. 3D printed tablets (Printlets) with braille and moon patterns for visually impaired patients. Pharmaceutics 12 (2), 1–14. https://doi.org/10.3390/pharmaceutics12020172.

Bhardwaj, U., Burgess, D.J., 2010. A novel USP apparatus 4 based release testing method for dispersed systems. Int. J. Pharm. 388 (1–2), 287–294. https://doi.org/10.1016/j.ijpharm.2010.01.009.

Carlier, E., Marquette, S., Peerboom, C., Denis, L., Benali, S., Raquez, J.-M., Amighi, K., Goole, J., 2019. Investigation of the parameters used in fused deposition modeling of poly (lactic acid) to optimize 3D printing sessions. Int. J. Pharm. 565, 367–377.

Cheng, L., Guo, S., Wu, W., 2009. Characterization and in vitro release of praziquantel from poly(ε-caprolactone) implants. Int. J. Pharm. 377 (1–2), 112–119. https://doi.org/10.1016/j.ijpharm.2009.05.007.

Darville, N., van Heerden, M., Vynckier, A.n., De Meulder, M., Sterkens, P., Annaert, P., Van den Mooter, G., 2014. Intramuscular administration of paliperidone palmitate extended-release injectable microsuspension induces a subclinical inflammatory reaction modulating the pharmacokinetics in rats. Pharm. Drug. Deliv. Pharm. Technol. 103 (7), 2072–2087.

Dissolution Methods Database | FDA. https://www.fda.gov/drugs/drug-approvals-and-databases/dissolution-methods-database. Accessed January 29, 2021.

dos Santos, J., Deon, M., da Silva, G.S., Beck, R.C.R., 2021. Multiple variable effects in the customisation of fused deposition modelling 3D-printed medicines: a design of experiments (DoE) approach. Int. J. Pharm. 597 (February), 120331 https://doi.org/10.1016/j.ijpharm.2021.120331.

Elbadawi, M., Muñiz Castro, B., Gavins, F.K.H., et al., 2020. M3DISEEN: A novel machine learning approach for predicting the 3D printability of medicines. Int. J. Pharm. 2020;590(September):119837. doi:10.1016/j.ijpharm.2020.119837.

Fanous, M., Bitar, M., Gold, S., et al., 2021. Development of immediate release 3D-printed dosage forms for a poorly water-soluble drug by fused deposition modeling: Study of morphology, solid state and dissolution. Int. J. Pharm. 2021;599:120417. doi:10.1016/j.ijpharm.2021.120417.

Goyanes, A., Robles Martinez, P., Buanz, A., Basit, A.W., Gaisford, S., 2015. Effect of geometry on drug release from 3D printed tablets. Int. J. Pharm. 494 (2), 657–663.

Goyanes, A., Scarpa, M., Kamlow, M., Gaisford, S., Basit, A.W., Orlu, M., 2017. Patient acceptability of 3D printed medicines. Int. J. Pharm. 530 (1-2), 71–78.

Hoang Thi, T.H., Chai, F., Leprêtre, S., Blanchemain, N., Martel, B., Siepmann, F., Hildebrand, H.F., Siepmann, J., Flament, M.P., 2010. Bone implants modified with cyclodextrin: Study of drug release in bulk fluid and into agarose gel. Int. J. Pharm. 400 (1-2), 74–85.

Holländer, J., Genina, N., Jukarainen, H., Khajeheian, M., Rosling, A., Mäkilä, E., Sandler, N., 2016. Three-dimensional printed PCL-based implantable prototypes of medical devices for controlled drug delivery. J Pharm Sci. 105 (9), 2665–2676.

Hope, A., Wade, S.J., Aghmesheh, M., Vine, K.L., 2021. Localized delivery of immunotherapy via implantable scaffolds for breast cancer treatment. J Control Release 2022 (341), 399–413. https://doi.org/10.1016/j.jconrel.2021.11.043.

Kožák, J., Rabišková, M., Lamprecht, A., 2021. In-vitro drug release testing of parenteral formulations via an agarose gel envelope to closer mimic tissue firmness. Int. J. Pharm. 594 (November 2020) https://doi.org/10.1016/j.ijpharm.2020.120142.

Leng, D., Chen, H., Li, G., Guo, M., Zhu, Z., Xu, L.u., Wang, Y., 2014. Development and comparison of intramuscularly long-acting paliperidone palmitate nanosuspensions with different particle size. Int. J. Pharm. 472 (1-2), 380–385.

Li, C., Cheng, L., Zhang, Y., Guo, S., Wu, W., 2010. Effects of implant diameter, drug loading and end-capping on praziquantel release from PCL implants. Int. J. Pharm. 386 (1–2), 23–29. https://doi.org/10.1016/j.ijpharm.2009.10.046.

Li, DeXia, Guo, G., Fan, RangRang, Liang, J., Deng, X., Luo, F., Qian, ZhiYong, 2013. PLA/F68/Dexamethasone implants prepared by hot-melt extrusion for controlled release of anti-inflammatory drug to implantable medical devices: I. Preparation, characterization and hydrolytic degradation study. Int. J. Pharm. 441 (1-2), 365–372.

Li, DeXia, Guo, G., Deng, X., Fan, RangRang, Guo, QingFa, Fan, M., Liang, J., Luo, F., Qian, ZhiYong, 2013. PLA/PEG-PPG-PEG/Dexamethasone implant prepared by hot-melt extrusion for controlled release of immunosuppressive drug to implantable medical devices, part 2: in vivo evaluation. Drug. Deliv. 20 (3-4), 134–142.

Lin, W., Shen, H., Xu, G., Zhang, L., Fu, J., Deng, X., 2018. Single-layer temperature-adjusting transition method to improve the bond strength of 3D-printed PCL/PLA parts. Compos. Part A Appl. Sci. Manuf. 115, 22–30. https://doi.org/10.1016/j.compositesa.2018.09.008.

Lizambard, M., Menu, T., Fossart, M., et al., 2019. In-situ forming implants for the treatment of periodontal diseases: Simultaneous controlled release of an antiseptic and an anti-inflammatory drug, Int. J. Pharm. 572(October) (2019) 118833. doi:10.1016/j.ijpharm.2019.118833.

LLC N. *Ingeo ™ Biopolymer 4060D Technical Data Sheet.* Vol 201.; 2005.

Manini, G., Deldime, M., Benali, S., Raquez, J.-M., Goole, J., 2021. Long-acting implantable dosage forms containing paliperidone palmitate obtained by 3D printing. Int. J. Pharm. 603 (May), 120702 https://doi.org/10.1016/j.ijpharm.2021.120702.

Manini, G., Deldime, M., Benali, S., Raquez, J.-M., Goole, J., 2021. Long-acting implantable dosage forms containing paliperidone palmitate obtained by 3D printing. Int. J. Pharm. 603, 120702.

Muñiz Castro, B., Elbadawi, M., Ong, J.J., Pollard, T., Song, Z., Gaisford, S., Pérez, G., Basit, A.W., Cabalar, P., Goyanes, A., 2021. Machine learning predicts 3D printing performance of over 900 drug delivery systems. J. Control Release. 337, 530–545.

Nober, C., Manini, G., Carlier, E., Raquez, J.-M., Benali, S., Dubois, P., Amighi, K., Goole, J., 2019. Feasibility study into the potential use of fused-deposition modeling to manufacture 3D-printed enteric capsules in compounding pharmacies. Int. J. Pharm. 569, 118581.

Pereira, B.C., Isreb, A., Forbes, R.T., Dores, F., Habashy, R., Petit, J.-B., Alhnan, M.A., Oga, E.F., 2019. 'Temporary plasticiser': a novel solution to fabricate 3D printed patient-centred cardiovascular 'polypill' architectures. Eur. J. Pharm. Biopharm. 135, 94–103.

Pires, F.Q., Alves-Silva, I., Pinho, L.A.G., et al., 2020. Predictive models of FDM 3D printing using experimental design based on pharmaceutical requirements for tablet production. Int. J. Pharm. 2020;588(July):119728. doi:10.1016/j.ijpharm.2020.119728.

Sadia, M., Arafat, B., Ahmed, W., Forbes, R., Alhnan, M., 2017. Channelled tablets: an innovative approach to accelerating drug release from 3D printed tablets. J Control Release. 2018 (269), 355–363. https://doi.org/10.1016/j.jconrel.2017.11.022.

Scoutaris, N., Ross, S.A., Douroumis, D., 2018. 3D printed "Starmix" drug loaded dosage forms for paediatric applications. Pharm Res. 35 (2).

Stewart, S.A., Domínguez-Robles, J., McIlorum, V.J., Gonzalez, Z., Utomo, E., Mancuso, E., Lamprou, D.A., Donnelly, R.F., Larrañeta, E., 2020. Poly(caprolactone)-based coatings on 3D-printed biodegradable implants: a novel strategy to prolong delivery of hydrophilic drugs. Mol. Pharm. 17 (9), 3487–3500.

Stewart, S., Domínguez-Robles, J., McIlorum, V., Mancuso, E., Lamprou, D., Donnelly, R., Larrañeta, E., 2020. Development of a biodegradable subcutaneous implant for prolonged drug delivery using 3D printing. Pharmaceutics. 12 (2), 105.

Thakkar, R., Pillai, A.R., Zhang, J., Zhang, Y., Kulkarni, V., Maniruzzaman, M., 2020. Novel on-demand 3-dimensional (3D) printed tablets using fill density as an effective release-controlling Tool. Polymers (Basel) 1–21.

Xu, X., Goyanes, A., Trenfield, S.J., et al., 2021. Stereolithography (SLA) 3D printing of a bladder device for intravesical drug delivery. Mater Sci Eng C. 2021;120(November 2020):111773. doi:10.1016/j.msec.2020.111773.

Zhang, B., Nasereddin, J., McDonagh, T., von Zeppelin, D., Gleadall, A., Alqahtani, F., Bibb, R., Belton, P., Qi, S., 2021. Effects of porosity on drug release kinetics of swellable and erodible porous pharmaceutical solid dosage forms fabricated by hot melt droplet deposition 3D printing. Int. J. Pharm. 604, 120626.

Zhang, J., Thakkar, R., Zhang, Y., Maniruzzaman, M., 2020. Structure-function correlation and personalized 3D printed tablets using a quality by design (QbD) approach. Int. J. Pharm. 590 (August), 119945 https://doi.org/10.1016/j.ijpharm.2020.119945.